Quantitative modeling of modulated ion injections observed by Polar-Thermal Ion Dynamics Experiment in the cusp region

D. C. Delcourt

Centre d'étude des Environnements Terrestre et Planétaires, Saint-Maur-des-Fossés, France

T. E. Moore, B. L. Giles, and M.-C. Fok

NASA Goddard Space Flight Center, Greenbelt, Maryland

Abstract. On May 13, 1996, as the Polar spacecraft was traveling at high invariant latitudes (~78°-79°) in the prenoon sector (~1050 magnetic local time), the Thermal Ion Dynamics Experiment on board recorded successive injections of protons with clear energy-time dispersion. These dispersion structures spread over several minutes and extend from several hundreds of eV down to a few tens of eV. During this pass, simultaneous measurements from the Wind spacecraft revealed little variation of the solar wind dynamical pressure but a gradual turning of the interplanetary magnetic field (IMF) from an essentially dawn-to-dusk orientation (i.e., predominant positive B_Y component and slightly negative B_Z) to a north-to-south one (predominant negative B_Z). We show that the observed injections result from magnetosheath particle entry at higher and higher latitudes in the dawn sector. Using test particle calculations in a simple model of reconnected interplanetary and magnetospheric field, we show that the injection modulation likely follows from changes in the dynamical regime experienced by the ions upon traversal of the magnetopause current sheet. That is, as the IMF gradually rotates, the time-varying B_Y and B_Z lead to changes in the adiabaticity parameter κ in the region of entry and affect particle access to the Polar location. In the morning sector where magnetosheath plasma accelerates downtail, such an access to the inner magnetosphere requires magnetic moment damping and is thus favored during nonadiabatic episodes. The flux variations obtained numerically are in qualitative agreement with those observed, both in terms of characteristic energy and overall time evolution. This supports our interpretation of the modulated ion injections in terms of intermittent nonadiabatic entry from the magnetosheath followed by time of flight dispersion between the magnetopause and the spacecraft.

1. Introduction

During magnetic field line reconnection [*Dungey*, 1961], magnetosheath plasma gains access to the high-latitude magnetosphere in the dayside sector. When the interplanetary magnetic field (IMF) is southward, this plasma entry occurs in the subsolar region equatorward of the magnetic cusp [e.g., *Hill and Reiff*, 1977; *Sonnerup et al.*, 1981; *Gosling et al.*, 1990], whereas for northward IMF in situ measurements provide evidences of plasma injection both equatorward and poleward of the cusp [e.g., *Fuselier et al.*, 1997; *Chandler et al.*, 1999]. These magnetosheath particles flowing along open magnetic field lines form a significant source of plasma for the magnetosphere. They give rise to the so-called plasma mantle at high latitudes [*Rosenbauer et al.*, 1975] and eventually flow into the distant magnetotail [e.g., *Pilipp and Morfill*, 1978]. In some instances, magnetic reconnection occurs in an intermittent manner, giving rise to transient plasma injections viewed as flux transfer events (FTE) [*Russell and Elphic*, 1979]. Expected signatures of such FTEs are, for example, abrupt discontinuities in the incoming ion characteristics [e.g., *Escoubet et al.*, 1992; *Lockwood et al.*, 1993] or the development of enhanced convection channels in the ionosphere [e.g., *Elphic et al.*, 1990; *Lockwood et al.*, 1990; *Pinnock et al.*, 1993]. Other observations provide evidences of quasi-steady reconnection between the IMF and the magnetospheric field, allowing more

continuous inflow of magnetosheath material [e.g., *Onsager et al.*, 1995; *Xue et al.*, 1997; *Trattner et al.*, 1999].

In their analysis of DMSP measurements at low altitudes in the cusp region, *Newell et al.* [1991] identified two distinct domains of downflowing magnetosheath particles during southward IMF. One, referred to as the cusp proper, corresponds to plasma entering through the frontside magnetopause at low latitudes. In this region of space, one has $\mathbf{J}.\mathbf{E} > 0$ (denoting by $\mathbf{E}$ and $\mathbf{J}$ the electric field and current, respectively) so that magnetosheath particles experience large (up to several keVs) acceleration at entry into the magnetosphere. Upon reaching low altitudes, these accelerated particles exhibit a pronounced dispersion characterized by decreasing energy with increasing latitude due to $\mathbf{E}\times\mathbf{B}$ filtering during transport [e.g., *Reiff et al.*, 1977]. The second domain of *Newell et al.* [1991] coincides with the plasma mantle and encompasses magnetosheath particles penetrating at high latitudes. These particles are decelerated ($\mathbf{J}.\mathbf{E} < 0$) at entry into the magnetosphere and give rise to a precipitating population (referred to as "cusp plume") in the hundreds of eV range just poleward of the cusp proper. Such an overall structure of precipitation in the high-latitude dayside sector was successfully modeled by *Onsager et al.* [1993].

In this study, we examine data obtained by the Thermal Ion Dynamics Experiment (TIDE) on board Polar in the vicinity of the dayside cusp in the late morning sector. These data display successive ion injections in the hundred of eV range. We analyze these observations with the help of numerical simulations that reconstruct the particle transport in realistic geomagnetic conditions. We show that the observed injections likely consist of magnetosheath ions penetrating through the dawn flank of the magnetosphere. We suggest that the injection modulation directly follows from the nonlinear dynamics of ions in the magnetopause current sheet. Such an interpretation based on changing dynamical regimes along steadily open magnetospheric field lines is at variance with scenarios based on transient reconnection as envisaged, for instance, by *Lockwood et al.* [1998]. In section 2 we will first describe the Polar-TIDE observations. In section 3 we will review some aspects of the magnetosheath ion dynamics at entry into the magnetosphere. In section 4 we will describe the modeling technique adopted, and the results of the numerical simulations will finally be discussed in section 5.

2. Observations

The Polar spacecraft was launched on February 24, 1996, onto an eccentric orbit with 86° inclination and apogee at 9 R_E geocentric distance. The TIDE instrument onboard this spacecraft is an ion mass spectrometer that provides three-dimensional distributions of major ion species in the 0-450 eV energy range above the spacecraft potential in one spin period, that is, every 6 s (see *Moore et al.* [1995] for a detailed description of the instrument). In Plate 1, we show H^+ measurements obtained on May 13, 1996, while Polar was traveling at an altitude of ~6 R_E from low to high latitudes in the prenoon sector. Top and bottom panels in this plate show spin-time and energy-time spectrograms, respectively, the H^+ flux being coded according to the color scale at left. In the top panel, plus and minus signs show the spin angles corresponding to ion motion along and against the magnetic field, respectively, whereas crosses show spin angles corresponding to the spacecraft direction of motion.

In the bottom panel of Plate 1, repeated injections of protons can be seen which exhibit clear energy-time dispersion. That is,

following a preliminary flux enhancement at ~0057 UT, a large dispersion structure is noticeable between ~0100 and ~0107 UT, the ion energy varying from above 400 eV down to a few tens of eV. From ~0107 UT, another dispersion trace can be seen with similar energy variation over most of the TIDE energy range. Owing to the large and variable magnetosheath fluxes present, the Toroidal Imaging Mass-Angle Spectrograph on board Polar which records ions in the ~30 eV-30 keV range did not provide continuous measurements during this event. However, the sparse data available exhibit trends similar to those of TIDE. Simultaneously, it can be seen in the top panel of Plate 1 that the injections are centered onto plus signs, thus consisting of ions that flow downward into the ionosphere. Gradual "C-like" deviations from the field direction are also noticeable in this panel which indicates that, as the energy decreases, the flow occurs in a more oblique direction.

A sample of these TIDE data with a higher time resolution is shown in Plate 2 which presents spin-energy spectrograms obtained from a given channel of the instrument during a three-spin period. Here again, plus and minus signs correspond to ion motion along and against the magnetic field, respectively. In the top panel of Plate 2 which displays measurements at ~0103 UT, that is, well inside the large dispersion structure in Plate 1, it is apparent that ions with larger energies have larger pitch angles. A quite similar behavior can be seen in the bottom panel of Plate 2 which shows the TIDE measurements obtained somewhat later (~0105 UT). Such an energy-pitch angle variation is a characteristic feature of ion injection in the dayside cusp region and results from time of flight effects between the source at the magnetopause and the spacecraft [e.g., *Burch et al.*, 1982]. On the other hand, the repeated occurrence of large-scale energy-time dispersion in Plate 1 suggests that this plasma source at high altitudes operates in an intermittent manner.

Information on the solar wind conditions prevailing during this pass can be obtained from Figure 1 which shows selected measurements from the Wind spacecraft. For the time interval considered (0030-0100 UT), Wind was located upstream of the magnetosphere at an X_{GSM} distance of ~27 R_E. The two top panels of Figure 1 show the GSM Y and Z components of the IMF as a function of time. It is apparent from these panels that the IMF is gradually rotating from a predominantly duskward orientation toward a predominantly southward one, B_Y tending toward zero (from positive values) and B_Z becoming increasingly negative. Still, abrupt B_Z jumps (a few nanoteslas) are noticeable at ~0045 and ~0050 UT, that are correlated with jumps in B_X (not shown). Simultaneously, in the three bottom panels of Figure 1 it can be seen that the solar wind ion density, velocity, and temperature are fairly steady throughout the time interval considered, with $N \approx 4.5$ cm^{-3}, $V \approx 360$ km s^{-1}, and $T \approx 4.5$ eV.

It was mentioned above that, during the pass shown in Plate 1, Polar was located in the prenoon sector. To get further insights into the regions of the magnetosphere that are connected to Polar during this pass, magnetic field lines that thread the spacecraft were traced using the model of Tsyganenko 1996 [see *Tsyganenko*, 1995] (hereinafter referred to as T-96). This semiempirical model uses as input the geodipole tilt angle, the solar wind dynamical pressure, the IMF B_Y and B_Z components as well as *Dst* index. Field line tracing was performed using actual values of these input parameters (Figure 1) and including an average propagation time of ~8 min from the Wind spacecraft. The results of these calculations are presented in Figure 2 which shows the magnetic field line projections in the *Y-Z* and *X-Z* planes. The various grey levels in this figure correspond to distinct

times between 0050 and 0108 UT, separated by steps of 20 s. It can be seen in Figure 2 that, throughout this pass, Polar was located on magnetic field lines that extend into the magnetosheath and which intercept the magnetopause near the terminator in the morning sector. As the spacecraft travels poleward and the IMF gradually rotates from an essentially duskward to southward orientation, the magnetopause crossing point is located at higher and higher latitudes but remains in the vicinity of the terminator.

3. Particle Dynamics at Entry Into the Magnetosphere

Figure 2 suggests that during the May 13, 1996 pass, Polar is exposed to magnetosheath particles penetrating into the magnetosphere through the dawn flank, that is, in a region where one has $\mathbf{J}.\mathbf{E} < 0$ in a like manner to the cusp plume of *Newell et al.* [1991]. Because the solar wind plasma parameters are remarkably steady during this event, we are led to examine whether IMF variations can be at the origin of the injections in Plate 1. To do so, it is necessary to further examine the dynamics of magnetosheath ions as they travel through the magnetopause current sheet. In this regard, it is apparent from the right panel of Figure 2 that, in the terminator region, magnetic field lines exhibit a sharp kink which can lead to breaking of adiabaticity if curvature and ion Larmor radii are of the same order of magnitude. A parameter which is frequently used to characterize the motion of charged particles in a field reversal is that introduced by *Büchner and Zelenyi* [1989], namely,

$$\kappa = \sqrt{\frac{R_C}{\rho_L}} \tag{1}$$

where R_C is the minimum curvature radius and ρ_L is the maximum Larmor radius. For $\kappa > 3$ the particle motion is adiabatic (magnetic moment conserving) and the guiding center approximation is valid. For κ of the order of 1 to 3, particles can be subjected to prominent magnetic moment scattering and their motion cannot be characterized by any invariant. Finally, for $\kappa < 1$, particles may experience meandering motion inside the field reversal as initially shown by *Speiser* [1965]. As will be seen in the following section, quantitative calculation for magnetosheath protons with a typical energy of 300 eV along the magnetic field lines shown in Figure 2 yields a κ parameter between ~1.5 and ~2 at the magnetopause. Within T-96 we may accordingly expect significant scattering of the magnetosheath H^+ upon entry into the magnetosphere.

On the other hand, nonlinear dynamics of the magnetosheath particles is here complicated by the fact that IMF B_Y is nonzero. Indeed, the above ordering of dynamical regimes based on the κ parameter corresponds to the $B_Y = 0$ limit in a one-dimensional field reversal, and nonzero B_Y can significantly alter this picture [e.g., *Zhu and Parks*, 1993]. As a matter of fact, *Delcourt et al.* [2000] demonstrated that, for nonzero B_Y and given value of κ, the amount of magnetic moment (μ) scattering critically depends upon the direction of propagation of the particles inside the field reversal. Equivalently, for given κ and given direction of propagation, μ scattering is contingent upon the sign of B_Y. It was shown by *Delcourt et al.* [2000] that this effect can be viewed as the result of a rapid rotation of the centrifugal impulse that perturbs the particle gyromotion near the field minimum. The nonadiabatic particle behavior is attenuated or enhanced when this

rotation opposes or goes together with the gyromotion, respectively.

To illustrate this effect, Figure 3 shows an example of H^+ trajectories entering from the magnetosheath into the magnetosphere for two opposite orientations of the IMF B_Y component. These ion trajectories were computed using the T-96 model and without taking into account the large-scale convection electric field. In the magnetosheath, test protons were initialized on the same magnetic field line anchored into the ionosphere at 75° invariant latitude (ILAT) and 1200 magnetic local time (MLT), assuming $\kappa = 1.5$ and a pitch angle of 10°. Different phases of gyration were also considered, varied from 0° to 360° by steps of 45°. The top panels of Figure 3 show the H^+ trajectory projection in the *Y-Z* plane (as viewed from the Sun), whereas the bottom panels present the particle magnetic moment as a function of time (as measured from that of magnetopause crossing). Considering first the case with IMF $B_Y < 0$ (right panels of Figure 3), it can be seen that, despite their relatively small initial pitch angle, the magnetosheath originating protons do not penetrate deeply into the magnetosphere as a result of large μ enhancements upon crossing of the magnetopause. Note in particular that these μ enhancements are of the same order of magnitude (about a factor 10) regardless of gyration phase. This behavior sharply contrasts with that displayed in the left panels of Figure 3 where IMF $B_Y > 0$. In this latter case, the net μ change experienced by the particles strongly depends upon gyration phase. Some ions exhibit μ enhancement by a factor of ~5 while others are subjected to μ damping. As a result of this, it can be seen in the upper left panel of Figure 3 that the test protons either mirror at high altitudes or penetrate down to low altitudes.

A more comprehensive view of the nonadiabatic ion behavior in Figure 3 can be obtained from Figure 4 which presents the net magnetic moment variations for a variety of initial pitch angles in the magnetosheath (the other initial parameters being unchanged). Like in Figure 3, left and right panels of Figure 4 correspond to opposite orientations of the IMF B_Y component. As a first comment, it can be seen in Figure 4 that, regardless of the sign of B_Y, μ variations are organized according to three distinct branches as is the case for $B_Y = 0$ [e.g., *Delcourt and Martin*, 1994], namely, systematic μ enhancements at small pitch angles, negligible μ changes at large pitch angles, and in between either μ enhancement or damping depending upon gyration phase. Still, as put forward by *Delcourt et al.* [2000], a striking feature in Figure 4 is that, even though initial conditions in the magnetosheath are identical, the three-branch pattern of μ variations is shifted toward small pitch angles for IMF $B_Y > 0$ (left panel) and toward large pitch angles for IMF $B_Y < 0$ (right panel). As an example, protons with 10° initial pitch angle experience a gyrophase dependent μ change in the former case and systematic μ enhancement in the latter, as is illustrated in Figure 3. Figure 4 accordingly demonstrates that, upon entry into the magnetosphere, the domain of velocity space that is affected by magnetic moment scattering possibly depends upon the orientation of the IMF B_Y component. In particular, since the vertical branch in Figure 4 spreads over a wider volume when $B_Y < 0$, a larger number of particles are then subjected to μ damping. Under the assumption of isotropic flux in the magnetosheath, this would lead to a more efficient filling of the loss cone and subsequent precipitation into the ionosphere.

4. Modeling Technique

To examine the relationship between nonlinear ion dynamics at entry into the magnetosphere and the May 13, 1996, observations of Plate 1, we performed test particle trajectory calculations in a field model reproducing the geomagnetic conditions of that day. Because a large number of test protons were necessary to sample the observations and because the T-96 model coupled with a three-dimensional description of the geoelectric field leads to prohibitive computation times, we did not use T-96 to reconstruct the full magnetosheath ion transport. Rather, we adopted a method similar to that used by *Curran and Goertz* [1989] to investigate particle distribution in a reconnection field geometry. That is, particles were traced in a simple model of the magnetopause current sheet which has characteristics similar to those in T-96. Energy-time spectrograms at the Polar location were subsequently reconstructed by applying Liouville theorem to a prescribed H^+ population in the magnetosheath and taking into account time delay for propagation from the magnetopause to the spacecraft. For the field reversal at the magnetopause, a one-dimensional parabolic model was used, the general expression of which in an arbitrary Cartesian coordinate system (I, J, K) is

$$\mathbf{B} = B_I \frac{K}{T} \mathbf{i} + B_J \mathbf{j} + B_K \mathbf{k}. \qquad (2)$$

Here T is a reference scale length representing the half-thickness of the current sheet, while $\mathbf{i}$, $\mathbf{j}$, and $\mathbf{k}$ are unit vectors in the I, J, and K directions, respectively. As mentioned above, the different parameters in (2) were varied so as to reproduce the time evolution of the magnetopause field reversal in T-96. This evolution can be better appreciated in Figure 5 which shows the propagated IMF B_Y and B_Z components, the field line inclination ($\delta = \arctan[-B_Z/B_Y]$) and field magnitude at the magnetopause, as well as the κ parameter of 300 eV protons as a function of time. In the top panels of Figure 5, one recognizes the IMF variations of Figure 1 with simultaneous B_Y and B_Z decreases punctuated by abrupt B_Z jumps. These B_Y and B_Z variations lead to a gradual increase of the field line inclination in Figure 5c. As for the κ profile in Figure 5e, it is of particular interest as it displays repeated increases from small (~1.5) to large (> 2) values. These κ variations are directly correlated with those of B_Z (Figure 5b). They suggest that inflowing magnetosheath protons are successively subjected to strongly and weakly nonadiabatic regimes.

As discussed in section 3, it should be kept in mind that a transverse component such as B_J in (2) causes magnetic moment scattering to depend upon the direction of propagation in the field reversal (for given B_J) or, alternatively, to depend upon the sign of B_J (for given direction of propagation). Conversely, if μ scattering in the field reversal does not depend upon the direction of propagation, one may conclude that $B_J = 0$ [see, e.g., *Delcourt et al.*, 2000, Figure 5]. It was shown in Figure 4 that, at 1200 MLT, radically different μ variations are obtained depending upon whether IMF B_Y is positive or negative, but it is not clear whether this is also the case near the terminator which is the region of interest in Plate 1. To examine this issue, we carried out selected trajectory computations along the T-96 field lines in Figure 2. At various times of the May 13, 1996, pass, test protons were launched from the magnetosheath with 300 eV energy and 1° pitch angle, considering different phases of gyration. The results of these calculations are shown in Figure 6 where the various solid lines depict the time evolution of the magnetic moment spread after entry into the magnetosphere. Because the test protons initially have small pitch angle, it can be seen in Figure 6 that they systematically experience μ increase upon crossing of the

magnetopause. As an example, ions entering at 0053 UT experience μ enhancements by a factor of ~100, whereas these μ enhancements reach ~400 at 0059 UT. Not surprisingly, comparison of Figures 5e and 6 reveals a $\Delta\mu$ evolution analogous to that of κ, with smaller or larger μ increases when κ departs from or tends toward unity, respectively. As for the dotted segments in Figure 6, they show the results obtained for the opposite IMF B_Y orientation. It is apparent that the μ changes achieved in this latter case are fairly similar to those in solid lines. As mentioned above, such an absence of asymmetry implies $B_J = 0$ in (2), and the field reversal in the terminator region can thus be simply described as

$$\mathbf{B} = B_I \frac{K}{T}\mathbf{i} + B_K\mathbf{k}. \qquad (3)$$

Particle tracing was carried out using (3) for the magnetopause field reversal with B_I, T, and B_K parameters evaluated from T-96 (namely, $B_K = B_{min}$ and $B_I/T = B_{min}/R_{C min}$, where B_{min} and $R_{C min}$ are the T-96 field magnitude and curvature radius at the magnetopause). In the computations, test protons were launched at different times with different energies and gyration phases from one edge of the current sheet (3), and they were traced backward in time until the other edge. During this transport, the convection electric field was accounted for in a manner similar to that of *Onsager et al.* [1995], namely, assuming that at equilibrium the magnetosheath bulk flow in the deHoffman-Teller frame is aligned at the magnetosheath Alfven speed V_A [*Cowley*, 1980]. This allows us to estimate the deHoffman-Teller frame velocity (i.e., the $\mathbf{E}\times\mathbf{B}$ drift speed) which varies in proportion to V_A. The H$^+$ distribution in the magnetosheath was taken as a flowing Maxwellian: $f \propto \exp[-(\mathbf{V}-\mathbf{V}_{bulk})^2/V_{th}^2]$ where $\mathbf{V}_{bulk}$ and V_{th} are the bulk and thermal speeds, respectively. As given by *Onsager et al.* [1995] (see, e.g., Figure 3 of that paper), plasma parameters in the magnetosheath were estimated from the gas-dynamic model of *Spreiter et al.* [1966]. In the terminator region and for the solar wind values shown in Figure 1, this model yields ~8 cm^{-3}, ~240 km s^{-1}, and ~56 eV for the magnetosheath ion number density, bulk speed, and temperature, respectively.

5. Numerical Results

Once all trajectory calculations were performed, energy-time spectrograms were reconstructed by weighting the test particles in the inflowing magnetosheath population and using Liouville theorem to infer the directional differential flux. Time delays were also included in order to account for ion propagation from the magnetopause to the spacecraft (separated by a curvilinear distance of ~16 R_E). The results of these simulations are presented in Plate 3 which shows the computed H$^+$ flux (color coded according to the scale at right) over a time interval similar to that in Plate 1. A striking feature in Plate 3 is the occurrence of repeated H$^+$ injections in the ~0.1-1.0 keV range. Like in Plate 1, these injections exhibit a clear energy-time dispersion that spreads over several minutes. The timing of these injections also resembles that in Plate 1 with onsets at ~0101 and ~0106 UT. On the whole the flux variations portrayed in Plate 3 are in qualitative agreement with those observed by Polar-TIDE, both in terms of characteristic energy and overall time evolution.

Data and simulations are more closely compared in Figure 7 which shows the overall dispersion traces obtained when low flux levels (smaller than 10% of the maximum value) are removed. In

this figure, some discrepancies between computations (hatched area) and observations (shaded area) are noticeable. In particular, the slopes of the various dispersion traces are somewhat different, and substantial overlapping of the computed traces can be seen, which is not the case in the TIDE data. It is likely that these deviations follow from the simplified model used to reconstruct the magnetosheath ion transport. For instance, unfolding of the particle pitch angle (due to magnetic moment conservation) between the magnetopause and the spacecraft is not accounted for in this model. Neither are the flux variations with pitch angle displayed in Plate 1. This directly affects the particle propagation time and consequently the overall structure of the dispersion pattern. The absence of overlapping in the TIDE data may suggest as well a separation between the magnetopause and the spacecraft that is somewhat smaller than that considered in the calculations. A shorter distance would indeed yield a harder slope of the computed dispersions and hence weaker overlapping. Keeping in mind these model limitations, the observed and computed structures in Figure 7 clearly bear some resemblance, with successive dispersion traces spreading over several minutes.

To further examine the origin of the injections in Plate 3, Figure 8 presents the average κ parameter, relative energy loss, and initial pitch angle in the magnetosheath as a function of energy and time. As noted earlier, the top panel of Figure 8 displays repeated sequences of low κ values that are directly correlated with the IMF B_Z jumps in Figure 5b (note that κ variations are here shifted in time as compared to Figure 5e due to propagation lag between the magnetopause and the spacecraft). By comparison with Plate 3, it can be seen that these episodes of low κ or, equivalently, of enhanced nonadiabaticity coincide with magnetosheath ion injections. The reason for this can be understood by looking at the pitch angle variations in the bottom panel of Figure 8. It can be seen in this panel that, at low energies, ions that reach Polar initially have small pitch angles in the magnetosheath. These ions travel adiabatically through the magnetopause current sheet and a small initial pitch angle is accordingly required to reach low altitudes. In contrast, at large energies (above ~100 eV), ions possibly behave in a nonadiabatic manner. In this case, ions which travel down to Polar are those which initially have large pitch angles and experience μ damping upon crossing of the magnetopause current sheet (in the middle panel of Figure 8, note the energy loss achieved during this crossing). In the morning sector, such ions that are scattered from large to small pitch angles carry substantial flux because the magnetosheath plasma accelerates downtail and flows in a direction relatively oblique to the magnetic field. Conversely, when κ increases and magnetic moment scattering weakens, a lesser flux is obtained in the parallel direction. It thus appears that it is the modulation of nonadiabatic ion behavior inside the magnetopause current sheet that is responsible for the repeated injections in Plate 3.

The present interpretation framework is at variance with that relating impulsive plasma injections to transient reconnection events [see, e.g., *Lockwood et al.*, 1998]. Here impulsive injections are rather viewed as the result of changes in the dynamical regime experienced by the ions as they flow along steadily open magnetic field lines. These injections follow from bursts of nonadiabaticity that favor the entry of magnetosheath population into the magnetosphere, the energy-time dispersion observed at the Polar location resulting from time of flight effects between the magnetopause and the spacecraft. This viewpoint is schematically summarized in Figure 9. In the top panel of this figure, it can be seen that, during adiabatic episodes, a limited amount of magnetosheath ions will enter into the magnetosphere

at small pitch angles and subsequently reach Polar. In contrast, during nonadiabatic episodes (bottom panel of Figure 9), ions that are nearly field-aligned in the magnetosphere originate from the core of the distribution in the magnetosheath. In essence, this mechanism is similar to that put forward in the inner plasma sheet [e.g., *Sergeev et al.*, 1983; *Zelenyi et al.*, 1990; *Delcourt et al.*, 1996] whereby chaotization of the ion motion in the transition region between taillike and dipolelike field lines leads to loss cone filling and subsequent precipitation into the auroral zone. *Sergeev et al.* [1993] argued that this mechanism may actually be responsible for the bulk of proton precipitation and identified the low-latitude edge of this precipitation as the onset of nonadiabatic motion in the magnetotail. The qualitative agreement between the TIDE observations (Plate 1) and the numerical simulations (Plate 3) suggests that such a nonadiabatic filling of the loss cone may similarly be at work at the magnetopause, but occurring in an intermittent manner due to fluctuations in the controlling IMF. The agreement between data and numerical results also suggests that the T-96 model used to constrain the simulations provides a relatively fair description of the open magnetosphere.

6. Conclusion

Analysis of the repeated ion injections observed by the TIDE intrument on board Polar on May 13, 1996, has led us to investigate the entry of magnetosheath plasma in the dawn magnetosphere. Using numerical calculations in a simple model of plasma transport that includes the full particle dynamics in the magnetopause current sheet and subsequent propagation to the spacecraft, we have shown that these injections may be due to changes in the dynamical regime experienced by the magnetosheath ions upon entry into the magnetosphere. Numerical simulations reveal that the IMF B_Y component can play a prominent role in this entry process, yielding either enhanced or attenuated changes of the particle magnetic moment, hence widely different mirroring altitudes. For the May 13, 1996, event, however, the IMF B_Z evolution appears more decisive for the inflowing ion dynamics. Because of intermittent decrease and increase of this IMF component, these ions are successively subjected to adiabatic and nonadiabatic regimes. Whereas weak penetration into the magnetosphere is achieved when the ions travel adiabatically, nonadiabatic behavior can lead to significant flux in the parallel direction via magnetic moment damping. Within the limits of the calculations, the flux variations obtained numerically are in qualitative agreement with those observed. Because of the short-lived character of the nonadiabatic episodes and propagation lag between the magnetopause and the spacecraft, high-energy particles are detected before the low-energy ones, leading to a pronounced energy-time dispersion at the Polar location.

References

Büchner, J., and L. M. Zelenyi, Regular and chaotic charged particle motion in magnetotaillike field reversals, 1, Basic theory of trapped motion, *J. Geophys. Res., 94*, 11,821, 1989.

Burch, J. L., P. H. Reiff, R. A. Heelis, J. D. Winningham, W. B. Hanson, C. Gurgiolo, J. D. Menietti, R. A. Hoffman, and J. N. Barfield, Plasma injection and transport in the mid-altitude polar cusp, *Geophys. Res. Lett., 9*, 921, 1982.

Chandler, M. O., S. A. Fuselier, M. Lockwood, and T. E. Moore, Evidence of component merging equatorward of the cusp, *J. Geophys. Res., 104*, 22,623, 1999.

Cowley, S. W. H., Plasma population in a simple open model magnetosphere, *Space Sci. Rev., 26*, 217, 1980.

Curran, D. B., and C. K. Goertz, Particle distribution in a two-dimensional reconnection field geometry, *J. Geophys. Res., 94*, 272, 1989.

Delcourt, D. C., and R. F. Martin Jr., Application of the centrifugal impulse model to particle motion in the near-Earth magnetotail, *J. Geophys. Res., 99*, 23,583, 1994.

Delcourt, D. C., J.-A. Sauvaud, R. F. Martin Jr., and T. E. Moore, On the nonadiabatic precipitation of ions from the near-Earth plasma sheet, *J. Geophys. Res., 101*, 17,409, 1996.

Delcourt, D. C., L. M. Zelenyi, and J.-A. Sauvaud, Magnetic moment scattering in a field reversal with nonzero B_Y component, *J. Geophys. Res., 105*, 349, 2000.

Dungey, J. W., Interplanetary field and the auroral zones, *Phys. Rev. Lett., 6*, 47, 1961.

Elphic, R. C., M. Lockwood, S. W. H. Cowley, and P. E. Sandholt, Flux transfer events at the magnetopause and in the ionosphere, *Geophys. Res. Lett., 17*, 2241, 1990.

Escoubet, C. P., M. F. Smith, S. F. Fung, P. C. Anderson, R. A. Hoffman, E. M. Basinska, and J. M. Bosqued, Staircase ion signature in the polar cusp: A case study, *Geophys. Res. Lett., 19*, 1735, 1992.

Fuselier, S. A., B. J. Anderson, and T. G. Onsager, Electron and ion signatures of field line topology at the low-shear magnetopause, *J. Geophys. Res., 102*, 4847, 1997.

Gosling, J. T., M. F. Thomsen, S. J. Bame, T. G. Onsager, and C. T. Russell, The electron edge of the low-latitude boundary layer during accelerated flow events, *Geophys. Res. Lett., 17*, 1833, 1990.

Hill, T. W., and P. H. Reiff, Evidence of magnetospheric cusp proton acceleration by magnetic merging at the dayside magnetopause, *J. Geophys. Res., 82*, 3623, 1977.

Lockwood, M., S. W. H. Cowley, P. E. Sandholt, and R. P. Lepping, The ionospheric signatures of flux transfer events and solar wind dynamic pressure changes, *J. Geophys. Res., 95*, 17,113, 1990.

Lockwood, M., W. F. Denig, A. D. Farmer, V. N. Davda, S. W. H. Cowley, and H. Lühr, Ionospheric signatures of pulsed magnetic reconnection at the Earth's magnetopause, *Nature, 361*, 424, 1993.

Lockwood, M., C. J. Davis, T. G. Onsager, and J. D. Scudder, Modelling signatures of pulsed magnetopause reconnection in cusp ion dispersion signatures seen at middle altitudes, *Geophys. Res. Lett., 25*, 591, 1998.

Moore, T. E., et al., The thermal ion dynamics experiment and plasma source instrument, *Space Sci. Rev., 71*, 409, 1995.

Newell, P. T., W. J. Burke, C.-I. Meng, E. R. Sanchez, and M. E. Greenspan, Identification and observations of the plasma mantle at low altitude, *J. Geophys. Res., 96*, 35, 1991.

Onsager, T. G., C. A. Kletzing, J. B. Austin, and H. MacKiernan, Model of magnetosheath plasma in the magnetosphere: Cusp and mantle particles at low-altitudes, *Geophys. Res. Lett., 20*, 479, 1993.

Onsager, T. G., S.-W. Chang, J. D. Perez, J. B. Austin, and L. X. Janoo, Low-altitude observations and modeling of quasi-steady magnetopause reconnection, *J. Geophys. Res., 100*, 11,831, 1995.

Pilipp, W. G., and G. Morfill, The formation of the plasma sheet resulting from plasma mantle dynamics, *J. Geophys. Res., 83*, 5670, 1978.

Pinnock, M., A. S. Rodger, J. R. Dudeney, K. B. Baker, P. T. Newell, R. A. Greenwald, and M. E. Greenspan, Observations of an enhanced convection channel in the cusp ionosphere, *J. Geophys. Res., 98*, 3767, 1993.

Reiff, P. H., T. W. Hill, and J. L. Burch, Solar wind plasma injection at the dayside magnetospheric cusp, *J. Geophys. Res., 82*, 479, 1977.

Rosenbauer, H., H. Grünwaldt, M. D. Montgomery, G. Paschmann, and N. Sckopke, Helios 2 plasma observations in the distant polar magnetosphere: The plasma mantle, *J. Geophys. Res., 80*, 2723, 1975.

Russell, C. T., and R. C. Elphic, ISEE observations of flux transfer events at the dayside magnetopause, *Geophys. Res. Lett., 6*, 33, 1979.

Sergeev, V. A., E. M. Sazhina, N. A. Tsyganenko, J. A. Lundblad, and F. Soraas, Pitch-angle scattering of energetic protons in the magnetotail current sheet as the dominant source of their isotropic precipitation into the nightside ionosphere, *Planet. Space Sci., 31*, 1147, 1983.

Sergeev, V. A., M. Malkov, and K. Mursula, Testing the isotropic boundary algorithm method to evaluate the magnetic field configuration in the tail, *J. Geophys. Res., 98*, 7609, 1993.

Sonnerup, B. U. Ö., G. Paschmann, I. Papamastorakis, N. Sckopke, G. Haerendel, S. J. Bame, J. R. Asbridge, J. T Gosling, and C. T. Russell, Evidence of magnetic field reconnection at the Earth's magnetopause, *J. Geophys. Res., 86*, 10,049, 1981.

Speiser, T. W., Particle trajectory in model current sheets, 1, Analytical solutions, *J. Geophys. Res., 70*, 4219, 1965.

Spreiter, J. R., A. Y. Alksne, and B. Abraham-Shrauner, Theoretical proton velocity distributions in the flow around the magnetosphere, *Planet. Space Sci., 14*, 1207, 1966.

Trattner, K. J., S. A. Fuselier, W. K. Peterson, J.-A. Sauvaud, H. Stenuit, N. Dubouloz, and R. A. Kovrazhkin, On spatial and temporal structures in the cusp, *J. Geophys. Res., 104*, 28,411, 1999.

Tsyganenko, N. A., Modeling the Earth's magnetospheric magnetic field confined within a realistic magnetopause, *J. Geophys. Res., 100*, 5599, 1995.

Xue, S., P. H. Reiff, and T. G. Onsager, Mid-altitude modeling of cusp ion injection under steady and varying conditions, *Geophys. Res. Lett., 24*, 2275, 1997.

Zelenyi, L. M., A. Galeev, and C. F. Kennel, Ion precipitation from the inner plasma sheet due to stochastic diffusion, *J. Geophys. Res., 95*, 3871, 1990.

Zhu, Z., and G. Parks, Particle orbits in model current sheets with a nonzero B_Y component, *J. Geophys. Res., 98*, 7603, 1993.

_____

  D. C. Delcourt, Centre d'étude des Environnements Terrestre et Planétaires, Centre National de la Recherche Scientifique, 4, Avenue de Neptune, 94107 Saint-Maur-des-Fossés, France. (delcourt@cetp.ipsl.fr)

  M.-C. Fok, B. L. Giles, T. E. Moore, NASA Goddard Space Flight Center, Interplanetary Physics Branch, Mail Code 692, Greenbelt, MD 20771 USA. (mei-ching.fok @ gsfc.nasa.gov; barbara.giles@gsfc.nasa.gov; thomas.e.moore@gsfc.nasa.gov)

Copyright 2000 by the American Geophysical Union.

Plate 1. (top) Spin angle-time spectrogram and (bottom) energy-time spectrogram recorded by the TIDE instrument on board Polar on May 13, 1996. Data are integrated over energy in the top panel and integrated over angle in the bottom panel. Plus and minus signs in the top panel indicate ion flows along and against the magnetic field, respectively. Crosses show the spacecraft direction of motion.

Plate 2. Spin angle-energy spectrogram recorded by TIDE during a three spin period at (top) ~0103 UT and (bottom) ~0105 UT. Plus and minus signs and crosses have the same definitions as in Plate 1.

Plate 3. Computed energy-time spectrogram for the May 13, 1996, event. The H^+ flux is coded according to the color scale at right and normalized to the maximum value. The white dashed line shows the upper limit of the TIDE instrument energy range.

Figure 1. Selected parameters recorded by the Wind spacecraft on May 13, 1996: (top to bottom) IMF B_Y component, IMF B_Z component, ion density, velocity, and temperature.

Figure 2. Magnetic field lines threading the Polar spacecraft from 0050 until 0108 UT on May 13, 1996, as obtained from T-96: (left) in the *Y-Z* plane, (right) in the *X-Z* plane. The various grey levels correspond to distinct times (separated by steps of 20 s).

Figure 3. Examples of H^+ trajectories in the T-96 model considering opposite orientations of the IMF B_Y component (namely, positive and negative in the left and right panels, respectively). The top panels show the trajectory projections in the *Y-Z* plane, whereas the bottom panels show the H^+ magnetic moment (normalized to the initial value) as a function of time (as measured from that of magnetopause crossing). In both cases the κ parameter is set to 1.5 and the test protons are launched along the magnetic field line anchored at 1200 MLT and 75° ILAT in the ionosphere. Dotted lines in the top panels indicate selected magnetic field lines at 75° ILAT.

Figure 4. H^+ magnetic moment (normalized to the initial value) after entry into the magnetosphere as a function of initial pitch angle in the magnetosheath. Like in Figure 3, the test protons have $\kappa = 1.5$ and are launched along the magnetic field line anchored at 1200 MLT and 75° ILAT in the ionosphere. Left and right panels relate to opposite orientations of the IMF B_Y component. The various dots in each panel correspond to different initial phases of gyration in the magnetosheath.

Figure 5. Selected parameters of the magnetic field geometry shown in Figure 2: (top to bottom) IMF B_Y and B_Z components (including propagation lag from the Wind spacecraft), magnetic field line inclination at the magnetopause, magnetic field magnitude at the magnetopause, and κ parameter of 300 eV protons.
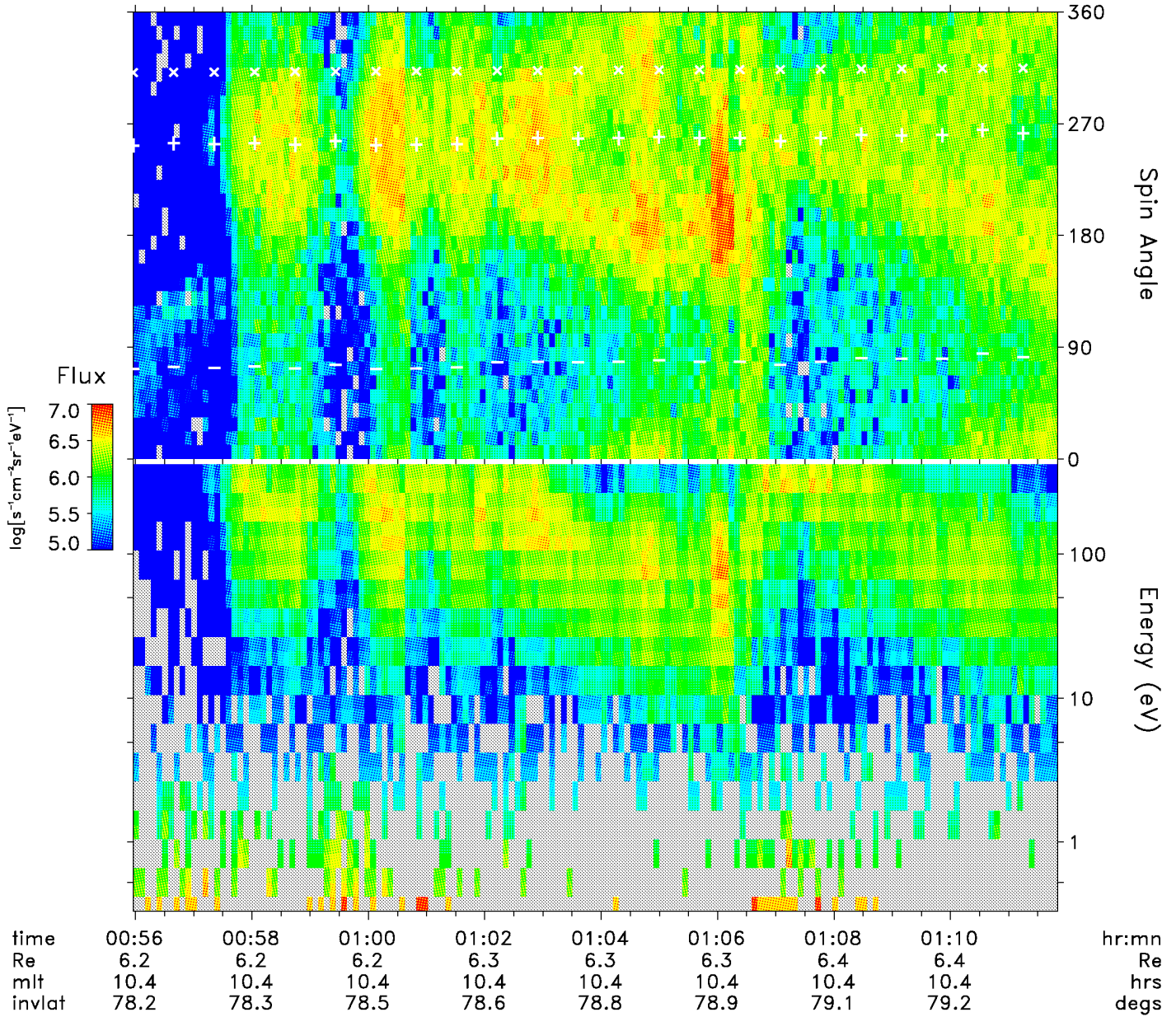
Figure 6. H^+ magnetic moment after entry into the magnetosphere (normalized to initial value in the magnetosheath) as a function of time for the magnetic field geometry shown in Figure 2. Test protons are launched from the magnetosheath with 1° pitch angle and different phases of gyration. The solid lines present the spread in final magnetic moment considering a positive IMF B_Y (as is the case in Figure 2), whereas the dotted lines show the results obtained for the opposite IMF B_Y orientation.

Figure 7. Observed (shaded) and computed (hatched) dispersion traces when low (< 10% of the maximum value) flux levels are removed.

Figure 8. Computed spectrograms showing (top) the average κ parameter, (middle) the relative energy change (defined as $\left| \varepsilon_{msphere} - \varepsilon_{msheath} \right| / \varepsilon_{msphere}$ where $\varepsilon_{msphere}$ and $\varepsilon_{msheath}$ denote H^+ energies in the magnetosphere and in the magnetosheath, respectively), and (bottom) the initial pitch angle in the magnetosheath. These different parameters are coded according to the grey scales at right.

Figure 9. Schematic representation of the magnetosheath ion population that can reach the Polar location depending upon whether the motion is (top) adiabatic or (bottom) nonadiabatic at entry into the dawn magnetosphere.

POLAR TIDE   05/13/96

Flux

log[s⁻¹cm⁻²sr⁻¹eV⁻¹]

Spin Angle

Energy (eV)

time	00:56	00:58	01:00	01:02	01:04	01:06	01:08	01:10	hr:mn
Re	6.2	6.2	6.2	6.3	6.3	6.3	6.4	6.4	Re
mlt	10.4	10.4	10.4	10.4	10.4	10.4	10.4	10.4	hrs
invlat	78.2	78.3	78.5	78.6	78.8	78.9	79.1	79.2	degs

POLAR TIDE 05/13/96

Energy Flux

$\log[eVs^{-1}cm^{-2}sr^{-1}eV^{-1}]$

8.0
7.5
7.0
6.5
6.0

01:03 UT

01:05 UT

Energy   1   10   100

MAGNETOSHEATH

MAGNETOSPHERE

$V_\perp$

$V_\parallel$

POLAR

NONADIABATIC

$V_\perp$

$V_\parallel$

POLAR

ADIABATIC